Appl. Phys. B 92, 295–302 (2008)
DOI: 10.1007/s00340-008-3075-6

Applied Physics B
Lasers and Optics

A. AMEDIEK✉
A. FIX
M. WIRTH
G. EHRET

Development of an OPO system at 1.57 μm for integrated path DIAL measurement of atmospheric carbon dioxide

Deutsches Zentrum für Luft- und Raumfahrt (DLR) Oberpfaffenhofen, Institut für Physik der Atmosphäre, 82234 Wessling, Germany

Received: 13 November 2007 / Revised version: 19 Mai 2008
Published online: 27 June 2008 •

ABSTRACT Active remote sensing is a promising technique to close the gaps that exist in global measurement of atmospheric carbon dioxide sources, sinks and fluxes. Several approaches are currently under development. Here, an experimental setup of an integrated path differential absorption lidar (IPDA) is presented, operating at 1.57 μm using direct detection. An injection seeded KTP-OPO system pumped by a Nd:YAG laser serves as the transmitter. The seed laser is actively stabilized by means of a CO_2 reference cell. The line-narrowed OPO radiation yields a high spectral purity, which is measured by means of a long path absorption cell. First measurements of diurnal variations of the atmospheric CO_2 mixing ratio using a topographic target were performed and show good agreement compared to simultaneously taken measurements of an in situ device. A further result is that the required power reference measurement of each laser pulse in combination with the spatial beam quality is a critical point of this method. The system described can serve as a testbed for further investigations of special features of the IPDA technique.

PACS 42.65.Yj; 42.68.Wt; 92.60.hg

1 Introduction

One of the most important topics in earth system science today is the investigation of the global carbon cycle. Identification of sources and sinks of atmospheric carbon dioxide is a matter of special importance herein [1, 2]. However, the spatial resolution of the existing global CO_2 network which is based on about 100 measurement sites monitoring local CO_2 concentrations with in situ techniques is not sufficient for detailed analysis [3]. Remote sensing from space is a promising approach to close the gaps [4]. Active remote sensing can complement passive sensors that have disadvantages due to interference of atmospheric aerosol [5], lack in global coverage, or low sensitivity near the earth's surface [6]. Furthermore, pulsed active systems allow precise determination of the column height. However, active systems are not yet well developed with regard to CO_2 measurements. This can partly be attributed to the very stringent requirements on measurement accuracy below 3–4 ppmv in CO_2 volume mixing ratio [7, 8]. This corresponds to a precision of about one order of magnitude higher compared to existing active systems for measuring atmospheric constituents, such as water vapor, ozone, or methane [9].

Current developments of pulsed systems for CO_2 measurements are described by Koch et al. [10] and Gibert et al. [11]. They report on test measurements with systems at a wavelength of 2 μm using heterodyne detection. Ismail et al. [12] developed a 2-μm system with direct detection. Systems based on continuous wave lasers are described by Spiers et al. [13] (2 μm, heterodyne detection) and Krainak et al. [14] (1.57 μm, direct detection). Early approaches are described by Bufton et al. [15] and Sugimoto et al. [16]. None of the systems mentioned has demonstrated the required accuracy yet. Hence the development of new systems using several methods of resolution is necessary.

Against this background we developed and demonstrated an experimental setup of an IPDA system for column content measurements of atmospheric carbon dioxide. The idea was the use of an injection seeded optical parametric oscillator (OPO) system as light source with potassium titanyl phosphate (KTP) as the non-linear medium. The basic principle of using pulsed laser light at 1.57 μm wavelength with a direct detection system, which was chosen within this study, has to our knowledge not yet been described. We investigate if such a system is able to achieve the stringent accuracy requirements.

We assume that our approach of a lidar system is able to achieve high measurement accuracy due to the fact that the chosen wavelength range allows for the use of state-of-the-art detectors that provide high sensitivity and that pulsed light ensures precise determination of range. Furthermore the direct detection approach avoids problems with speckle noise in contrast to heterodyne detection [4].

This paper reports on the setup of the developed system, its special properties and results of first test measurements that were performed using a horizontal absorption path with a topographic target (trees) in the distance of 2 km.

2 IPDA principle

The IPDA technique also known as hard-target lidar is a special case of differential absorption lidar (DIAL) [9, 13]. Instead of atmospheric backscatter the return of a hard

✉ Fax: +49-8153-281271, E-mail: axel.amediek@dlr.de

target, such as vegetation, buildings, water or clouds, etc., is used. The target reflex offers the great advantage of this method of a very strong backscatter signal which allows high measurement sensitivity. However, any profile information is lost.

The received power P of a hard target reflex (assuming Lambertian scattering) is given by [17]:

$$P = \frac{\varrho}{\pi}\frac{E}{t_{\mathrm{eff}}}\frac{A}{R^2}T_{\mathrm{opt}}T_{\mathrm{atm}}\exp\left(-2\int_0^R N_{\mathrm{CO_2}}(r)\sigma(\lambda, r)\,\mathrm{d}r\right), \quad (1)$$

with the target reflectance ϱ, the laser pulse energy E, the effective pulse length of the received laser pulse t_{eff} [7], the receiver telescope area A, the distance R between system and target, the overall optical transmission of the receiver system T_{opt}, the optical transmission due to other atmospheric constituents T_{atm}, the number density of CO_2 molecules $N_{\mathrm{CO_2}}$ at the position r, and the absorption cross section σ of CO_2 at a given wavelength λ at the position r. The absorption cross section is calculated on the basis of a Voigt profile [18] that represents the absorption line shape under atmospheric conditions.

The relation between the powers of the received online and offline target reflex pulses $P_{\mathrm{on}}/P_{\mathrm{off}}$ using (1) leads to:

$$\int_0^R N_{\mathrm{CO_2}}(r)\,\Delta\sigma(r)\,\mathrm{d}r = \frac{1}{2}\ln\frac{P_{\mathrm{off}}}{P_{\mathrm{on}}}. \quad (2)$$

The differential absorption cross section is given by $\Delta\sigma = \sigma(\lambda_{\mathrm{on}}) - \sigma(\lambda_{\mathrm{off}})$, at which λ_{on} and λ_{off} correspond to wavelengths with molecular absorption (online) and without absorption (offline), respectively.

The column averaged CO_2 mixing ratio $q_{\mathrm{CO_2}}$ is defined by:

$$q_{\mathrm{CO_2}} = \frac{\int_0^R N_{\mathrm{CO_2}}(r)\,\mathrm{d}r}{\int_0^R N_{\mathrm{air}}(r)\,\mathrm{d}r}, \quad (3)$$

with the number density of (moist) air N_{air}. The following expression results from (2) in the case of a horizontal path, at which $\Delta\sigma$ is constant over r :

$$q_{\mathrm{CO_2}} = \frac{1}{2N_{\mathrm{air}}\Delta\sigma R}\ln\left(\frac{P_{\mathrm{off}}}{P_{\mathrm{on}}}\right). \quad (4)$$

Equation (4) is used for the data interpretation of the measurement results shown below.

3 Experimental set-up

Figure 1 shows the principle of the setup. Special features are a two-wavelength injection seeded OPO system providing alternating two narrow-band wavelengths around 1.57 μm, a stabilized online wavelength via reference cell, a spectral purity control via multipass cell, a spectrum analyzer, and a direct detection receiver system with power reference measurement of each outgoing laser pulse. All main properties are listed in Table 1. The CO_2 absorption line used (online: 1572.993 nm, offline: 1573.16 nm) provides almost no interference to atmospheric water vapor and shows low temperature dependence of the absorption cross section. The online and offline wavelengths were selected by means of numerical simulations based on the absorption line parameters of the HITRAN 96 database [19].

The OPO system [20] acts as a tunable frequency converter to generate the desired wavelengths. The fundamental (1064 nm) of an injection seeded, Q-switched and flash lamp-pumped Nd:YAG laser (Continuum NY-61) serves as the pump radiation for the OPO [21]. The OPO is designed as a ring cavity to avoid back reflections that may introduce spectral instabilities or damage to the seed lasers. In combination with the distributed feedback (DFB) seed lasers that were

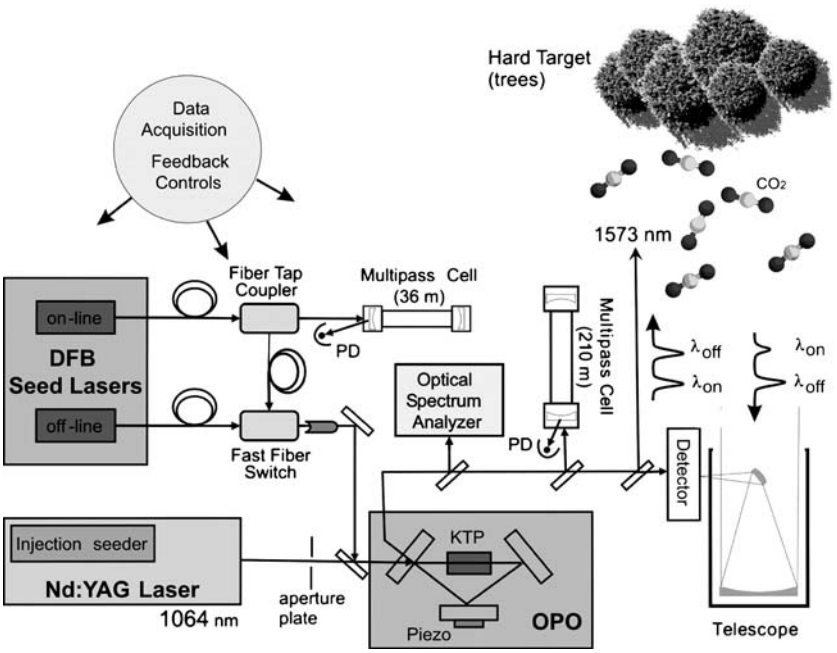

FIGURE 1 Schematic of experimental setup

Transmitter	
Pump source	Flash lamp pumped, Q-switched Nd:YAG with integrated injection seeder
Pump wavelength	1064 nm
Repetition rate	10 Hz
Incident pump energy for OPO	70–100 mJ per pulse
Pulse length	8 ns
OPO	
Ring cavity length (optical)	92 mm
Non-linear medium	KTP, $(5 \times 5 \times 20)$ mm^3, $\vartheta = 90°$, $\varphi = 0°$
Phase-matching scheme	Non-critical
Output energy	10 mJ per pulse
Output wavelength	1572.1 to 1574.6 nm
Pulse length	5 ns
Bandwidth (unseeded)	0.2 nm (FWHM)
Threshold	55 mJ unseeded, 40 mJ seeded
Injection seeding	
Seed laser	DFB telecom diode laser, fiber coupled
Online wavelength	1572.993 nm
Offline wavelength	1573.16 nm
Data rate (online/offline pulse pairs)	5 Hz
Receiver	
Telescope	Newtonian, 15 cm diameter
Field of view	≈ 4 mrad
Detector	InGaAs-PIN (Hamamatsu G8605, Active area ∅ 1 mm)
Data acquisition	12-bit, 400 MHz

TABLE 1 Technical data of the CO_2-IPDA system

used for the injection seeding it was not necessary to use additional protection like a Faraday isolator. KTP was selected as non-linear medium because of its favorable properties [22]. A non-critical phase-matching scheme is used [23]. The cavity length is fine-tuned via a piezo element. The cavity mirrors are embedded in a solid aluminum block, leading to a good passive stability of the OPO. The generated signal radiation (1.57 μm) serves as measurement radiation, whereas the idler radiation at 3.3 μm is not used.

Figure 2 shows the longitudinal mode structure of the OPO: During this measurement the wavelength of the online seed laser was continuously tuned. The increase of the OPO output power during the resonance of the seed laser, at which the injection seeding is active, represents the OPO modes. The relative frequency was identified by means of the signal of a Fabry–Pérot interferometer (FPI). The distance between two peaks corresponds to twice the cavity length, because a double circulation in the cavity occurs. It was possible to reduce the in-between modes by adjustment of the cavity, but a complete suppression of this occurrence could not be achieved. Figure 4 depicts the dependence of the OPO output energy on the pump energy. The conversion efficiency is about 10%. Since the output energy of 10 mJ per pulse was fully sufficient further optimization of the OPO's efficiency was not undertaken. Figure 4 indicates that no saturation effects occur. The bandwidth of the free running OPO (without injection seeding) is about 0.2 nm FWHM. This is appropriate for the generation of the two defined wavelengths, online and offline (distance: 0.17 nm), by means of injection seeding, with a single OPO configuration.

By means of temperature tuning [23, 24] and non-collinear phase matching [23, 25] (tuning of the angle between pump

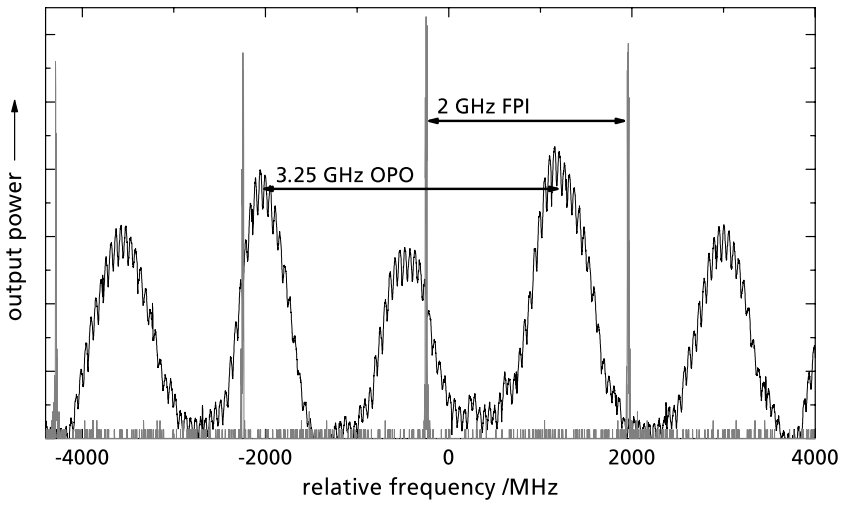

FIGURE 2 Measured longitudinal mode structure of the OPO. The increase of the OPO output power during seed laser resonance is displayed. Additionally the markers of the Fabry–Pérot interferometer (FPI) for relative wavelength calibration are shown

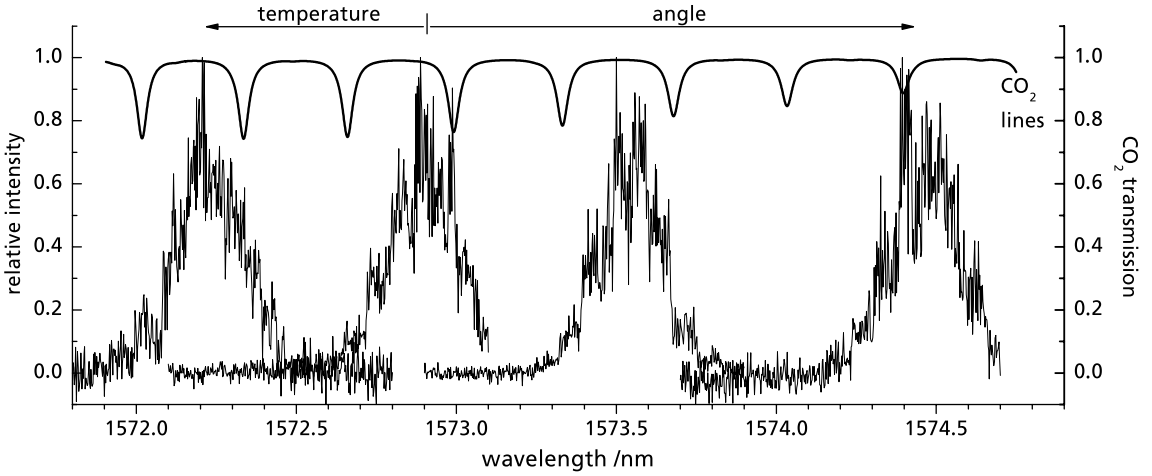

FIGURE 3 Tuning range of the OPO. Four of the possible OPO radiation spectra (unseeded) within the tuning range are displayed. The tuning was performed by means of temperature variation and non-collinear phase matching. Additionally matching CO_2 absorption lines (calculated using HITRAN) are shown

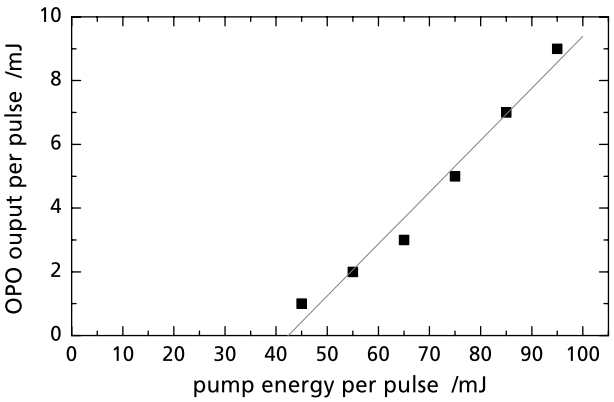

FIGURE 4 OPO output energy vs. pump energy

beam and signal beam) it was possible to fine-tune the bandwidth of the free running OPO and match to the defined online and offline wavelengths (see Figs. 3 and 5).

The method of injection seeding [26] provides the two defined narrow-band wavelengths that act as online and offline wavelengths, within the bandwidth of the free running OPO (see Fig. 5).

Seeding is performed by means of two fiber coupled commercially available telecom DFB diode lasers (Fujitsu FLD5F15CA-S9090), one for online and offline, respectively. Their radiation is alternately coupled to the OPO via a fast fiber switch (Agiltron "CrystaLatch") (Fig. 1). Switching is performed synchronously to the 10 Hz Nd:YAG pump laser pulses. So the effective measurement data rate is as high as 5 Hz. The DFB laser modules contain an optical isolator (22 dB) that protects against possibly remaining back reflections.

The absolute wavelength accuracy needed and the stability of the online seed laser are achieved by using a 36-m multipass absorption cell filled with pure CO_2 (10 hPa pressure) as the reference [27]. A very high slope of the absorption line's edge allows for a precise control loop. It was stabilized to the line center of the atmospheric pressure-broadened line. For that purpose a simple edge control was used, since the line maximum of the atmospheric line coincides with the edge of the reference cell's line, because of the pressure shift of the atmospheric absorption line compared to the reference cell's line. A precise knowledge of the pressure shift coefficient [28] is a precondition to avoid a wavelength bias. The offline seed laser was not actively stabilized due to its passive stability of better than 1.3 GHz (monitored by means of the spectrum analyzer), which leads to an error of below 0.1% in the case of the shown measurements.

Figure 6 shows the achieved stability of 5 MHz (rms) of the online seed laser. In the case of the shown measurements (horizontal path) an online stability of better than 70 MHz is needed to achieve an error of below 0.1%. It is assumed that there is no significant wavelength offset between the radiation of the seed laser and the radiation emitted by the OPO. An offset (for example due to cavity pulling if the cavity is slightly out-of-tune) can be measured and controlled by a heterodyne measurement (superposition of seed laser and OPO) [29, 30]. This approach was successfully tested, but not applied during the shown measurements.

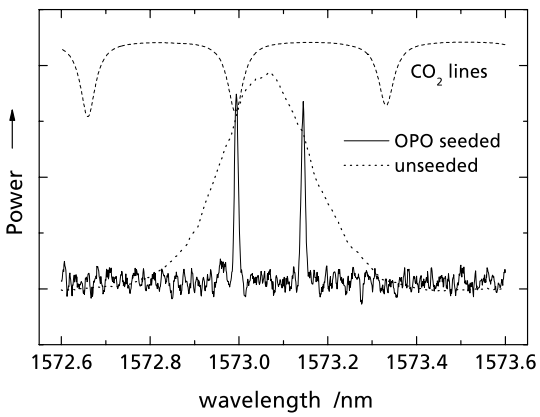

FIGURE 5 Spectra of the OPO radiation measured by means of an optical spectrum analyzer: narrow-band online and offline radiation during seeded operation (*straight line*), free running OPO without seeding (*dotted line*) and calculated CO_2 absorption lines (*dashed line*)

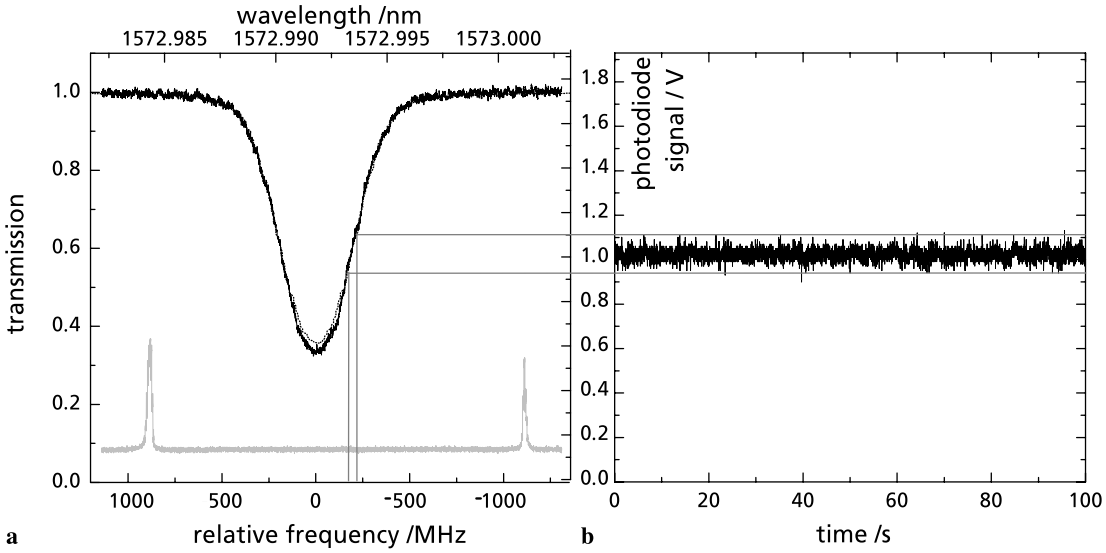

FIGURE 6 Online stabilization. (**a**) Absorption line scan of CO_2 (36-m multipass cell) at 10 hPa pressure (*straight line*), calculated line profile (*dotted line*), Fabry–Pérot interferometer markers for relative wavelength calibration (*grey*). (**b**) Time behavior of the stabilized online seeder: the relative frequency is deduced from the photodiode signal via the calibrated line scan. An accuracy of 5 MHz (rms) is achieved

It is crucial to ensure a sufficient high spectral purity [31] of the emitted online laser radiation. Otherwise the effective differential absorption of CO_2 was undefined, resulting in a large uncertainty in calculating its mixing ratio. In the case of the shown measurements a spectral purity of $\geq 99.9\%$ is needed to achieve a systematic error of $\leq 0.1\%$.

The spectral purity was determined by means of a long pass absorption cell (210 m) filled with pure CO_2 (35 hPa pressure). The strongly saturated absorption line acts as a highly wavelength-stable narrow-band filter (1.3 GHz FWHM). Spectral impurity due to OPO side modes or broadband emission can accurately be measured by means of this setup [27].

A spectral purity of the injection seeded OPO online radiation of as high as 99.9% was determined. The OPO cavity length was manually controlled via a piezo element (Fig. 1) to maintain a maximum spectral purity.

Figure 7 depicts the configuration that was used for the test measurements. A Newtonian telescope with a 15 cm diameter mirror was used to collect the backscattered light. The usage of the same detector for power reference and the target reflex measurements avoids variances in the response that may occur in the case of two detectors. The implementation of scattering disks that homogenize the light also plays a key role. It was not possible to achieve a signal that was sufficiently stable without these components. However, strong signal losses are the consequence.

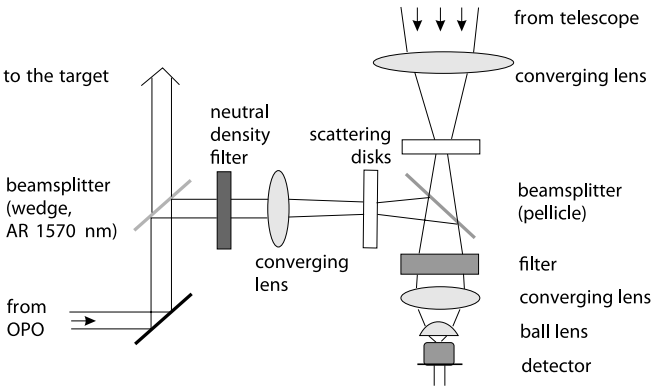

FIGURE 7 Setup of the receiving optics. The light collected by the telescope is homogenized by a scattering disc and focused on the detector. The power reference measurement is implemented by means of two beamsplitters that guide a small portion (homogenized by a second scattering disk) of the outgoing beam to the detector

A PIN diode was used as detector, although the usage of an APD is aspired due to the comparatively high sensitivity. However, APDs currently available have only very small active areas (about 0.2 mm diameter), requiring a more sophisticated focusing setup. Hence, in this first setup, the PIN diode was chosen.

4 Test measurements

4.1 *Configuration*

The test measurements were performed synchronously with the IPDA system and an in situ device (Carbondio, Pewatron AG, Switzerland), which detected the CO_2 mixing ratio of the air outside of the laboratory ($\sim$ 10 m above ground). It is calibrated by means of two gas mixtures with known CO_2 mixing ratios (air without CO_2 to set the zero-point and air containing 520 ppm CO_2 to calibrate the scale). The IPDA measurement runs along a 2 km horizontal path (about 10 m above ground) from the laboratory to a group of trees that act as a hard target. The surrounding area is rural and no notable local CO_2 sources are known.

Diurnal variations of the atmospheric CO_2 mixing ratio that naturally occur near the ground are measured. To get strong gradients of the mixing ratio the following special situation was chosen for measurement: the break-up of a ground inversion that is usually built up in spring and summer under cloudless conditions at night. In such an inversion layer the CO_2 that is mainly produced by vegetation accumulates near the ground during night and mixing ratios of up to 500 μmol/mol can be observed. When the solar driven atmo-

spheric convection starts in the morning, the mixing ratio falls to a comparatively low value.

4.2 *Results*

Figure 8 shows the temporal development of the CO_2 mixing ratio during 32 h. Because of the ground inversion high mixing ratios of up to 500 μmol/mol were measured at night time. The IPDA measurement shows very good agreement with the in situ data. The calculation of the CO_2 mixing ratio q_{CO_2} was done by using (4). To reduce the statistical error, 10 min averages were calculated. The "log after averaging" method [32] was used to avoid statistical biasing due to the non-linearity of the equation:

$$q_{CO_2} = \frac{1}{2N_{air}\Delta\sigma R} \ln\left(\frac{\sum_i (P_{off,i}/P^{ref}_{off,i})}{\sum_i (P_{on,i}/P^{ref}_{on,i})}\right), \quad (5)$$

where P_{on} is the power of the online target reflex, P_{off} the power of the offline target reflex, and P^{ref} are the corresponding power reference measurements. The calculation of $\Delta\sigma$ and N_{air} requires pressure and temperature data. These were obtained by the institute's meteorological station. The distance R to the target was determined from the pulse runtime with an accuracy of about 5 m.

Figure 9 shows the differences between IPDA lidar and in situ measurements. There are varying deviations with 2% (rms), plus constant biases. Characteristic of this setup are strong differences with respect to the amplitude of the bias occurring at different measurement runs. Measurement *a* represents a case with a small bias (2.2%) and measurement *b* a strong bias (9%).

In principle it is difficult to compare point measurements with column averaged measurements. So part of the deviations can be explained by the unequal volumes that are captured by the different measurement instrumentations. Nevertheless, even if all known parameters that limit the accuracy of the measurement are considered (wavelength accuracy and stability, spectral purity, temperature dependence, range determination, detector noise, line parameter, calibration error of the in situ device, variation of atmospheric water vapor content) it clearly appears that the occurred deviations can not be

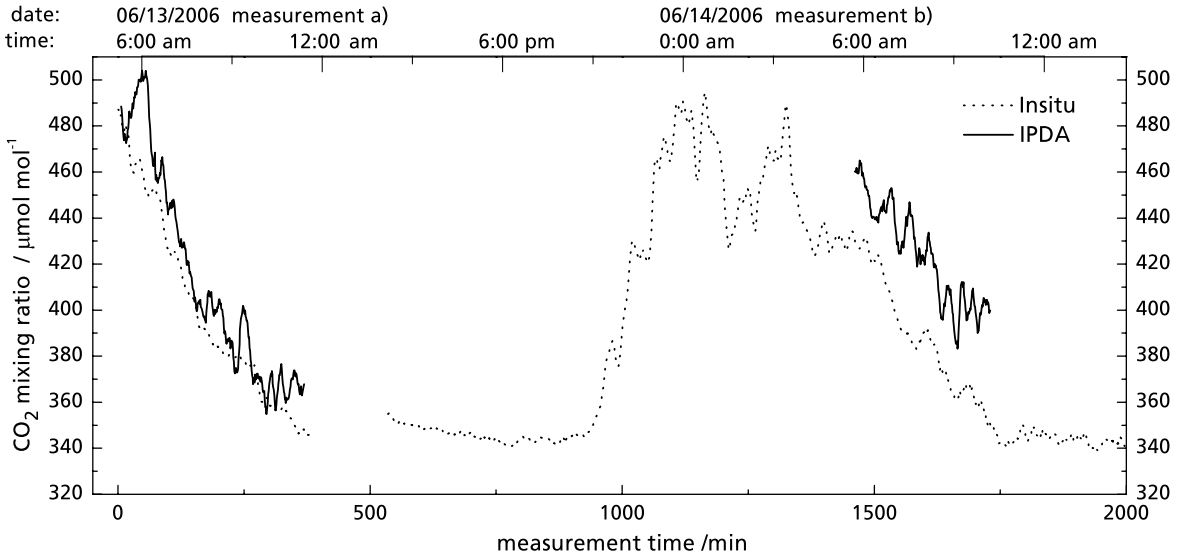

FIGURE 8 Simultaneous measurements of the diurnal variations of atmospheric CO_2 performed with the presented IPDA system and an in situ sensor

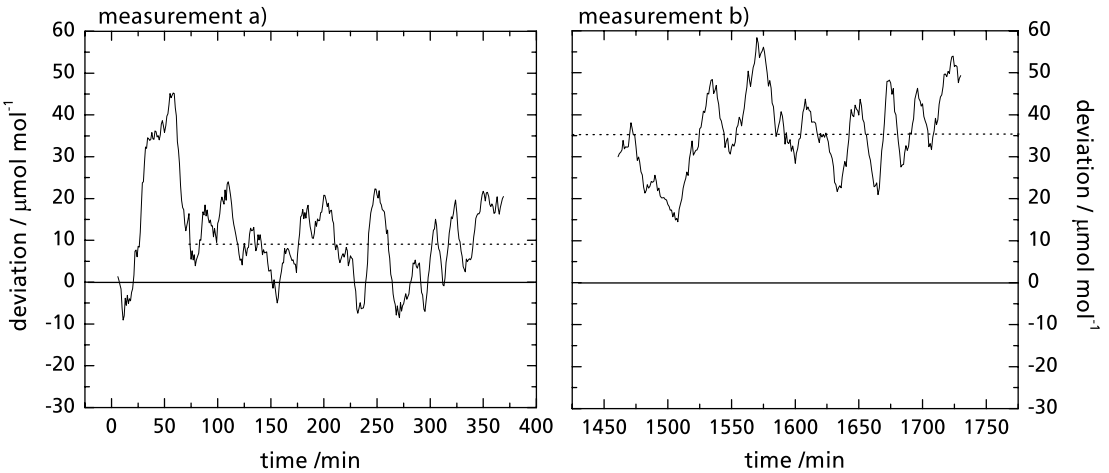

FIGURE 9 Measured deviation between IPDA system and in situ sensor for the measurement (**a**) and (**b**) depicted in Fig. 8

explained completely by this. In particular, the considerable difference in the biases of the measurements is noticeable, because in this case some of the typical sources of constant biases, such as uncertainties of the HITRAN line parameters, can not be the reason. Moreover it is implausible that the different methods (column measurement and point measurement) lead to constant biases over several hours. Considering the experience with the setup of the receiver optics it is most plausible that largely the power reference measurement and the focusing of the target reflex onto the detector in combination with the spatial quality of the beam causes the residual deviations.

5 Discussion

The described experimental setup has shown that it is possible to measure variations in the atmospheric CO_2 mixing ratio by means of an IPDA lidar using an OPO system as frequency converter for generation of 1.57 μm. The observed errors can be explained by an insufficiently accurate power reference measurement and precise focusing of the target reflex onto the detector. Scattering disks in the optical path enhance the stability of the signal, but lead to signal losses. Hence further optimizations of the receiver optics are necessary. To achieve an accurate power reference measurement seems to be a great challenge of the IPDA technique, if high measurement accuracy is required.

A very good spatial quality of the laser radiation is required to reach this aim. The described experimental setup shows deficiencies at this point. There are instabilities and inhomogeneities of the laser beam profile which in combination with a structured target might also lead to measurement errors. Within the scope of this work an optimization of this issue could not be performed. The variations in the M^2 of the OPO beam are still unknown. Instabilities of the pump laser and the observed double circulation are considered to belong to the reasons for an unstable spatial beam profile. Suggestions for the improvement of this first setup include the replacement of the currently used flash lamp pumped Nd:YAG laser by a more stable diode pumped system and the use of a telescope instead of an aperture plate for downsizing the pump beam diameter in front of the OPO.

Yet, the presented system has shown that the application of an OPO system as frequency converter for a CO_2 lidar transmitter is a promising approach. Using KTP as the non-linear medium and a pump wavelength of 1064 nm all suitable CO_2 absorption lines of the 1.57 and 1.6 μm bands are accessible: Using a non-critical phase-matching scheme 8 lines around 1.573 nm are accessible (Fig. 3) and, additionally, in the case of angle phase matching (tuning of the angle between pump beam and crystal) [23] the remaining lines are usable. In addition, it is possible to generate adequate output powers for measurements with a target distance of up to 10 km, while wavelength stability is very high. A spectral purity of as high as 99.9% is achieved. Due to the use of pulsed light a precise determination of the range is possible. All these points allow a measurement accuracy below 1%. One special issue of the IPDA technique that has to be analyzed in detail, is the investigation of effects due to spatially structured targets that, on a moving measurement platform, potentially could cause the introduction of systematic errors. The system described, with its short pulse length of 5 ns and its data acquisition sampling rate of 400 MHz, provides ideal conditions for such an analysis.

6 Summary

The experimental setup of an IPDA system for the measurement of atmospheric carbon dioxide using a topographic target was demonstrated. For the first time, measurements on the diurnal variations of CO_2 at 1.57 μm wavelength using a direct detection receiving system were performed. An OPO system with KTP as the non-linear medium and pumped by a Nd:YAG laser serves as light source. Alternating injection seeding via two telecom DFB laser diodes provides the required narrow-band online and offline wavelengths. An online seed laser stability of 5 MHz was accomplished by using a CO_2-filled 36 m multipass cell. A spectral purity of the OPO emitted radiation of as high as 99.9% was achieved, determined by a CO_2-filled long pass absorption cell.

Comparative measurements on the diurnal CO_2 variations performed by the IPDA lidar and an in situ device show good agreements.

The power reference measurement of each outgoing laser pulse, a special feature of IPDA systems, turned out to be a critical point of this technique. In addition there are highest requirements for the spatial beam quality and the receiving optics.

The presented system is suitable as a testbed for further investigations of special features of the IPDA technique and has the potential to significantly exceed the measurement accuracy shown in the first test case presented.

ACKNOWLEDGEMENTS The authors would like to thank Georg Simmet and the institute's mechanical workshop for technical support. Additionally we thank Hans Rüba and Andreas Petzold for providing the in situ device.

REFERENCES

1 S. Solomon, D. Qin, M. Manning, Z. Chen, M. Marquis, K.B. Averyt, M. Tignor, H.L. Miller, *IPCC 2007: Climate Change 2007: The Physical Science Basis* (Cambridge University Press, Cambridge, 2007)
2 S. Houweling, F.-M. Bréon, I. Aben, C. Rödenbeck, M. Gloor, M. Heimann, P. Ciais, Atmosph. Chem. Phys. **4**, 523 (2004)
3 C. Rödenbeck. S. Houweling, M. Gloor, M. Heimann, Atmosph. Chem. Phys. **3**, 1919 (2003)
4 G. Ehret, C. Kiemle, M. Wirth, A. Amediek, A. Fix, S. Houweling, Appl. Phys. B **90**, 593 (2008)
5 S. Houweling, W. Hartmann, I. Aben, H. Schrijver, J. Skidmore, G.J. Reolofs, F.M. Breon, Atmosph. Chem. Phys. **5**, 3003 (2005)
6 R.J. Engelen, G.L. Stephens, J. Appl. Met. **43**, 373 (2004)
7 G. Ehret, C. Kiemle, Final Report of ESA Study 10880/03/NL/FF (2005)
8 F.M. Bréon, P. Peylin, Final Report of ESA Study 15247/01/NL/MM (2003)
9 C. Weitkamp, *Lidar: Range Resolved Optical Remote Sensing of the Atmosphere* (Springer, Berlin Heidelberg New York, 2005)
10 G.J. Koch, B.W. Barnes, M. Petros, J.Y. Beyon, F. Amzajerdian, J. Yu, R.E. Davis, S. Ismail, S. Vay, M.J. Kavaya, U.N. Singh, Appl. Opt. **43**, 5092 (2004)
11 F. Gibert, P.H. Flamant, D. Bruneau, C. Loth, Appl. Opt. **45**, 4448 (2006)
12 S. Ismail, G.J. Koch, M.N. Abedin, T. Refaat, K. Davis, C. Miller, U.N. Singh, S. Vay, T. Mack, in *Proceedings of 23rd International Laser Radar Conference* (2006), pp. 349–352
13 G.D. Spiers, R.T. Menzies, D.M. Tratt, M. Phillips, in *Proceedings of 2nd Annual Earth Science Technology Conference* (NASA Earth Science Technology Office, Greenbelt, 2002)

14 M.A. Krainak, A.E. Andrews, G.R. Allan, J.F. Burris, H. Riris, X. Sun, J.B. Abshire, in *Conference on Lasers and Electro-Optics, CLEO '03* (2003)
15 J. L. Bufton. T. Itabe, L.L. Strow, C.L. Korb, B.M. Gentry, C.Y. Wenig, Appl. Opt. **22**, 2592 (1983)
16 N. Sugimoto, A. Minato, Appl. Opt. **32**/**33**, 6827 (1993)
17 W.B. Grant, Appl. Opt. **21**, 2390 (1982)
18 S. Ismail, E.V. Browell, Appl. Opt. **28**, 3603 (1989)
19 L.S. Rothman, C.P. Rinsland, A. Goldman, S.T. Massie, D.P. Edwards, J.M. Flaud, A. Perrin, C. Camy-Peyret, V. Dana, J.Y. Mandin, J. Schroeder, A. Mc-Cann, R.R. Gamache, R.B. Wattson, K. Yoshino, K. Chance, K. Jucks, L.R. Brown, V. Nemtchinov, P. Varanasi, J. Quant. Spectrosc. Radiat. Transf. **60**, 665 (1998)
20 C.L. Tang, W.R. Bosenberg, T. Ukachi, R.J. Lane, L.K. Cheng, IEEE Proc. **80**, 365 (1992)
21 G. Ehret, A. Fix, V. Weiß, G. Poberaj, T. Baumert, Appl. Phys. B **67**, 427 (1998)
22 J.T. Lin, Opt. Quantum Electron. **22**, 283 (1990)
23 F. Zernicke, J.E. Midwinter, *Applied Nonlinear Optics* (Wiley, New York, 1973)
24 K. Fradkin-Kashi, A. Arie, P. Urenski, G. Rosenman, Opt. Lett. **25**, 743 (2000)
25 N. Boeuf, D. Branning, I. Chaperot, E. Dauler, S. Guerin, G. Jaeger, A. Muller, A. Migdall, Opt. Eng. **39**, 1016 (2000)
26 J.E. Bjorkholm, H.G. Danielmeyer, Appl. Phys. Lett. **15**, 171 (1969)
27 G. Poberaj, A. Fix, A. Assion, M. Wirth, C. Kiemle, Appl. Phys. B **75**, 165 (2002)
28 J. Henningsen, H. Simonsen, J. Mol. Spectrosc. **203**, 16 (2000)
29 R.T. White, Y. He, B.J. Orr, M. Kono, K.G.H. Baldwin, Opt. Lett. **28**, 1248 (2003)
30 T. Schröder, C. Lemmerz, O. Reitebuch, M. Wirth, C. Wührer, R. Treichel, Appl. Phys. B **87**, 437 (2007)
31 T.J. Mckee, J. Lobin, W.A. Young, Appl. Opt. **21**, 725 (1982)
32 M.J.T. Milton, P.T. Woods, Appl. Opt. **26**, 2598 (1987)